Pandemic *Vibrio parahaemolyticus* wave succession by gene loss

Chao Yang[1,#*], Hongling Qiu[2,#], Sarah L. Svensson[1#], Chengpei Ni[3,#], Song Gao[3], Zhizhou Jia[1], Huiqi Wen[1], Li Xie[1], Wenxuan Xu[1], Yujiao Qin[1], Shuzhu Lin[1], Jiancheng Wang[1], Yiquan Zhang[4], Yinghui Li[5], Min Jiang[5], Xiaolu Shi[5], Qinghua Hu[5], Zhemin Zhou[6], Yanjie Chao[1], Ruifu Yang[7], Yujun Cui[7], Jaime Martinez-Urtaza[8,*], Hui Wang[2,*], Daniel Falush[1,*]

[1] The Center for Microbes, Development and Health, CAS Key Laboratory of Molecular Virology and Immunology, Shanghai Institute of Immunity and Infection, Chinese Academy of Sciences, Shanghai, China;

[2] School of Public Health, Shanghai Jiao Tong University School of Medicine, Shanghai, China;

[3] Wuxi Center for Disease Control and Prevention, Shenzhen, China;

[4] Department of Clinical Laboratory, Nantong Third People's Hospital, Affiliated Nantong Hospital 3 of Nantong University, Nantong, Jiangsu, China;

[5] Shenzhen Center for Disease Control and Prevention, Shenzhen, China;

[6] Key Laboratory of Alkene-Carbon Fibers-Based Technology & Application for Detection of Major Infectious Diseases, Cancer Institute, Suzhou Medical College, Soochow University, Suzhou, China;

[7] State Key Laboratory of Pathogen and Biosecurity, Beijing Institute of Microbiology and Epidemiology, Beijing, China;

[8] Department of Genetics and Microbiology, Facultat de Biociències, Universitat Autònoma de Barcelona, Barcelona, Spain

# These authors contributed equally to the article

* Corresponding authors:

C.Y.: cyang@siii.cas.cn; J.M.-U.: Jaime.Martinez.Urtaza@uab.cat;

H.W.: huiwang@shsmu.edu.cn; D.F.: daniel.falush@siii.cas.cn

Abstract

While the importance of spontaneous mutation and gene acquisition in the emergence and adaptive evolution of microbial pathogens is well recognized, the role of gene loss remains underexplored. Here, by large-scale phylogenomic analysis of 8,684 global isolates, we reconstructed the origin and evolutionary dynamics of the pandemic clone (PC) of *Vibrio parahaemolyticus*, the leading cause of seafood-associated infections worldwide. As has also been observed for the pandemic lineage of *V. cholerae*, there was an 'explosive' burst of gene and genomic island acquisition during the emergence of the clone followed by divergence into distinct, successive sublineages mediating waves of infections. In *V. parahaemolyticus*, a recent global wave succession event has been driven by gene-loss in the putrescine utilization (Puu) pathway, which confers phenotypic advantages related to environmental adaptation (enhanced biofilms) and human transmission (increased cell adhesion and intestinal colonization, reduced virulence in an animal model and milder clinical symptoms in humans), aligning with the trade-off hypothesis of pathogen virulence evolution. We identify similar lineage-specific Puu-gene-loss across multiple bacterial genera, with effects on biofilm and adhesion replicated in *V. cholerae* and *E. coli*, suggesting convergent evolution and universal mechanisms across bacteria. Our findings provide a novel paradigm of adaptative evolution by gene loss in a pandemic pathogen.

Introduction

Microbial pathogens have recurrently emerged from environments or animals, with a few leading to disease epidemics or pandemics that pose notable public health challenges[1,2]. Understanding the genetic basis of pathogen emergence and adaptive evolution is critical for disease control and prevention, especially for pandemic pathogens. *Vibrio*, Gram-negative, halophilic bacteria that are ubiquitous in marine and aquatic habitats, are ideal models for investigating pathogen emergence and evolution. Among >100 *Vibrio* species, approximately 12 cause human infections[3]. Two species, *V. cholerae* and *V. parahaemolyticus*, are associated with disease pandemics, with the ongoing seventh cholera pandemic attributed to El Tor (7PET) isolates. *V. cholerae* 7PET was inferred to originate from a pre-pandemic strain that subsequently underwent explosive diversification - gaining multiple genetic elements within a short timeframe (~15 years), including the El Tor type cholera toxin prophage and *Vibrio* seventh pandemic islands (VSP-I and VSP-II)[4,5]. During the seventh pandemic, three successive sub-lineages of 7PET were identified, corresponding to the three independent but overlapping waves of global transmission[5,6], which may be driven by antibiotic resistance[7].

V. parahaemolyticus is the leading cause of seafood associated infections worldwide, with an increase in incidence over the last two decades. Its geographical range has also been expanding, possibly due to global warming[3,8,9]. The emergence of pandemic clone (PC), characterized by serotype O3:K6, substantially changed the *V. parahaemolyticus* epidemiology[10–12]. The O3:K6 PC strain was first isolated in 1995 from a traveler returning to Japan from Indonesia, and in 1996, it caused a disease outbreak in Calcutta, India[10]. Subsequently, it rapidly spread worldwide and came to dominate infections in many regions, along with rapid antigenic divergence (49 serotypes reported)[10–12]. Molecular and epidemiological surveillances has provided evidence that the PC may have originated from a

serotype O3:K6 non-pathogenic strain, after acquisition of multiple marker genes (e.g. virulence regulatory gene sequence *toxRS/new*[13], phage f237 and its unique open reading frame *orf8*[14]), type 3 or 6 secretion systems (T3SS or T6SS) and several *V. parahaemolyticus* genomic islands (VPaI-1 to VPaI-7)[15,16]. However, how these events happened, the driving force and mechanism underlying these events remain unclear. Currently, there is a lack of comprehensive genomic view on the origin and evolution of the PC.

Leveraging a large-scale, global genome dataset of *V. parahaemolyticus*, we comprehensively reconstructed the evolutionary history of the PC. Intriguingly, we identified several similarities between PCs of *V. parahaemolyticus* and *V. cholerae*. However, distinct from *V. cholerae*, we found that gene loss has played a key role in the evolution of *V. parahaemolyticus* PC. We investigated the underlying molecular mechanisms of gene-loss medicated adaptation, and showed that it is likely universal among bacteria.

Results

From pre-pandemic (pre-PC) to PC

We assembled a total of 8,684 high-quality genomes of global *V. parahaemolyticus* isolates, including 333 newly sequenced and 8,351 publicly available genomes (**Supplementary Table 1**). To characterize population structure and identify PC isolates, we constructed a maximum-likelihood (ML) phylogenetic tree based on core-genome single-nucleotide polymorphisms (SNPs). Based on the ML tree and pairwise SNP-distance, 2,815 were assigned as PC isolates (mean SNP-distance: 437), 39 as pre-PC (close relatives of PC, mean SNP-distance to PC: 15,463), with the remaining being non-PC isolates (mean SNP-distance to PC: 55,554, **Fig. 1a**).

Pre-PC isolates were further split into four sub-groups, designated pre-PC1 to pre-PC4, respectively (**Fig. 1b,c**). Pre-PC1 to pre-PC3 were exclusively identified in Asia, with pre-PC1 and pre-PC2 being clinical isolates, while pre-PC3 were mainly environmental strains. The closest relative of the PC, pre-PC4, was represented mainly (13/16) by environmental isolates from Asia (Japan and China) and the US. The serotypes of most pre-PC isolates (33/39) were predicted to be O3:K6, and sequence types (STs) of pre-PC4b (a subset of pre-PC4) isolates were ST3 except one strain (**Fig. 1c** and **Supplementary Table 2**).

We identified a significant temporal signal among pre-PC3b to PC isolates and inferred the dated phylogeny (**Fig. 1b,2a**). The most recent common ancestor (MRCA) of the PC was estimated at 1983 (95% confidence interval [CI]: 1979-1985), 12 years preceding its first discovery in 1995. Early strains (eight strains isolated in 1996) exhibited substantial genomic diversity, with an average of 38 non-recombined SNPs, consistent with the long time-interval between origination and first discovery (**Fig. 2a**).

We investigated the distribution of known PC marker genes/islands and inferred the evolutionary history from pre-PC to PC (**Fig. 1b,c** and **Extended Data Fig. 1)**. The PC likely originated from a serotype O3:K6 pathogenic strain encoding T3SS1, T6SS2, phage f237 and VPaI-3, and subsequently acquired T6SS1 and the *toxRS/new* sequence. Interestingly, we

identified ‘explosive’ evolution defined as gain of multiple genes/islands within a short timeframe, as seen during the origin of *V. cholerae* 7PET. Between 1920 (MRCA of pre-PC4b and PC) and 1983 (MRCA-PC), MRCA-PC gained multiple dispersedly distributed genetic elements, including the well-known virulence factor thermostable direct hemolysin gene *tdh*, *orf8*, and six out of the seven VPaIs, along with 86 mutations and 80 homologous recombination events. Moreover, *trh* (*tdh*-related hemolysin), VPaI-1 and VPaI-2 were independently gained or lost by pre-PC strains.

We further investigated the source of these marker genes/islands by searching against non-PC genomes (**Extended Data Fig. 2**). All of them were identified in non-PC isolates with varying frequencies, indicating their sources are likely *V. parahaemolyticus*, rather than other *Vibrio* or bacteria. Moreover, the PC appeared to gain phage f237, VPaI-1 and VPaI-7 from non-PC strains, despite being encoded by pre-PC strains. Apart from marker genes/islands, six PC-specific genes were identified, three of which were within the superintegron (**Supplementary Table 3**).

Fine-scale population structure of PC

To reduce the effect of repeat sampling (strains from disease outbreaks) and exclude outlier strains, we generated a representative subset of 942 PC isolates for further analysis (see methods), spanning 20 countries across five continents between 1996 and 2022 (**Extended Data Fig. 3**). Among the representative isolates, we identified 26,377 core-genome SNPs, with 66% attributed to homologous recombination. Two recombination hotspots were identified, including the known O:K antigen region[17] and a novel hotspot (VP1883-1891) encoding a type II toxin-antitoxin system and cold shock protein. There were 281 homoplastic non-recombined SNPs, of which 26 were convergently identified 6-18 times in 16 genes associated with quorum sensing, environmental response and virulence (**Extended Data Fig. 4** and **Supplementary Table 4**).

We constructed an ML tree and dated phylogeny for PC representative strains (**Fig. 2a,b**). By integration with hierarchical clustering (**Extended Data Fig. 5**), we split the PC into four sub-lineages corresponding to waves of infections (**Fig. 2a-d**), which was also observed in the *V. cholerae* 7PET[5]. Following the nomenclature of *V. cholerae*, we designated these sub-lineages as wave-1 to 4, respectively. The estimated MRCA times for wave-1 to wave-3 were close (1984-1987), while wave-4 emerged more recently in 1998.

We identified 11 serotypes and three STs in representative strains (**Fig. 2b**). While O3:K6 was dominant (79%), serotype conversions were identified, particularly in wave-2 and wave-3. ST3 (96%) remained the predominant ST. Several marker genes/islands (VPaI-1, 4, 5 and *orf8*) were lost in 2%-8% of representative isolates, with the others being conserved (**Extended Data Fig. 6a**). Notably, the genomic island VPaI-7 encoding *tdh* and T3SS2 showed high differentiation between different waves (**Extended Data Fig. 6b**). Additionally, we observed a conserved antimicrobial resistance (AMR) gene profile (**Extended Data Fig. 6a**). Apart from intrinsic ampicillin resistance-related genes, no recently acquired gene was identified in >1% of representative isolates.

Wave succession and global transmission

Remarkably, we identified a 'wave succession' pattern: wave-1 to wave-4 succeeded each other temporally as the major wave (**Fig. 2c,d**). Wave-4 frequency has been increasing since its emergence, ultimately becoming predominant from 2012 onward. Wave succession was independently observed in multiple countries, including two well-sampled countries, China and the US. In most countries or regions, wave composition was diverse, except for two South American countries, Peru and Chile, where wave-1 has dominated for over a decade (**Fig. 2d**).

Since its origin, the effective population size (*Ne*) of the PC increased exponentially until 1998 (**Fig. 2e**). Subsequently, *Ne* fluctuated and showed a decreasing trend after 2010. Population dynamics of waves was consistent with temporal dynamics, with the *Ne* peaking alternatively for different waves. Post-2010, the *Ne* of wave-4 exceeded others and remained stable, while *Ne* of other waves declined rapidly.

We inferred the geographical transmission history of the PC by phylogeographical analysis, focusing on cross-continent events. A total of 67 transmission events were identified, mostly transient and not leading to local colonization (**Extended Data Fig. 7**). Only six 'TC' events (Transmissions resulting in local Colonization that persisted for ≥3 years) were identified (**Fig. 2b** and **Extended Data Fig. 7**). Wave-1 in South America likely sourced from a single TC event from Asia to Peru in 1990 (TC1), much earlier than its first discovery in South America (1997). Subsequently, wave-1 spread from Peru to Chile and backward transmissions were also identified (TC2-4). Additionally, two TC events from Asia to North America were identified (TC5-6) in other waves.

Effects of Puu-gene loss

Puu-gene loss associated with wave-4 replacement

To investigate the genetic basis of the wave-4 replacement of other waves, we comprehensively identified wave-4-specific variations and examined their functions. A total of 40 variations were identified (**Fig. 3a** and **Extended Data Table 1**), including 29 SNPs (located in 26 genes and 3 intergenic regions), two small indels (located in 2 genes) and most notably, the absence of nine adjacent genes (VP1775-VP1786) annotated to be involved in the putrescine utilization (Puu) pathway. The Puu-pathway degrades the polyamine putrescine into 4-aminobutanoate (GABA) or spermidine (**Fig. 3b**) and was reported to be related to putrescine catabolism in *Escherichia coli*[18] and biofilm formation in *Pseudomonas aeruginosa*[19].

Growth and biofilm formation

To validate the function of Puu-genes in *V. parahaemolyticus,* we generated deletion mutants for *puuA* (VP1781) and *puuC* (VP1776) in the wildtype strain RIMD2210633 (wave-3, hereafter RIMD-W3), expected to be defective in sub-pathway (SP) 1 and SP1-3, respectively (**Fig. 3b**). As reported in *E. coli*[18], both Δ*puuA* and Δ*puuC* exhibited deficient or reduced growth when putrescine served as the sole carbon or nitrogen source compared with the wildtype parental strain, with complementation of the deletion strains *in trans* (C-Δ*puuA* and

C-Δ*puuC*) restored growth (**Fig. 3c**). Moreover, both mutants showed enhanced biofilm formation under rich (alkaline peptone water, APW) or low-nutrition (M9 minimal) media with high (3%) or moderate (1%) salt concentrations after 48 hours of culture (**Fig. 3d** and **Extended Data Fig. 8**).

We further investigated the effect of Puu-gene-loss on metabolites by targeted metabolomics. We focused on low-nutrition and moderate-salt condition, where most significant biofilm differences were observed, while minimizing the interference from substances in complex media. As expected with Puu-gene-loss, there was a significant accumulation of extracellular putrescine (stationary phase) and reduced extracellular GABA levels (logarithmic and stationary phases) for both mutants, while no such difference was measured for intracellular levels. Intracellular spermidine was unexpectedly significantly reduced for both mutants during stationary phases (**Fig. 3e**).

Given consistent changes in metabolites (putrescine and GABA) during stationary phases, we further performed transcriptomic sequencing under this phase (13h) to identify differentially expressed genes (DEGs) that may underlie the Δ*puuA*/Δ*puuC* mutant phenotypes. We identified multiple DEGs between wildtype and mutants (WT *vs* M) associated with biofilm or biofilm-related pathways, including c-di-GMP, quorum sensing, CupE-fimbriae and Flp-pili (**Fig. 3f**, **Extended Data Fig. 9** and **Supplementary Table 5**). Moreover, we quantified c-di-GMP temporal dynamics by introducing dual-fluorescence reporter plasmids into wildtype and mutant strains. Consistent with transcriptomic results and higher biofilm formation, c-di-GMP levels were significantly higher in both mutants compared to wildtype in stationary phase (**Fig. 3g**).

To explore whether metabolites are drivers of phenotypes and gene expressions, we tested the effects of exogenous putrescine. Upon putrescine addition, both wildtype and mutants showed significantly increased biofilm and c-di-GMP levels (**Fig. 3b,g**). The effect of exogenous putrescine on global gene expressions was more pronounced in mutants than in wildtype, possibly due to the efficient putrescine turnover in the wildtype, as indicated by significant upregulation of Puu-genes upon addition of putrescine (**Extended Data Fig. 9**). Regardless of the degree of impact, multiple biofilm-related DEGs (WT *vs* M) were further significantly up- (e.g. *opaR*, *cusA-E* and *flp*) or down-regulated (e.g. *ompU*) in both wildtype and mutant strains when we added exogenous putrescine (**Fig. 3f** and **Extended Data Fig. 9**). Together, these findings indicate that increased extracellular putrescine caused by Puu-gene-loss enhances biofilms by regulating biofilm-related genes and promoting c-di-GMP synthesis.

Human-related phenotypes

The most significant category of DEGs (WT *vs* M) were those encoding CupE-fimbriae and Flp-pili. Adding exogenous putrescine further up-regulated *cusA-E* and *flp* in mutants, and also up-regulated *cusA* in wildtype (**Fig. 3f** and **Extended Data Fig. 9**). In addition to their role in biofilms, fimbriae and pili are generally related to cell adhesion for pathogens[20]. Motivated by these observations, we performed Caco-2 cell adhesion assays and found significantly enhanced adhesion by the mutants *vs.* wildtype (**Fig. 3h**). We also tested whether

increased cell adhesion transformed into enhanced intestinal colonization. We constructed bioluminescent wildtype and mutant strains and traced their colonization of mice after oral gavage using *in vivo* imaging. At 5 hours post-infection, mice infected with mutants exhibited markedly stronger luminescence compared to wildtype (**Fig. 3i**). Bacteria were then rapidly cleared in mice, no detectable luminescence was observed for wildtype and mutant strains by 10 hours post-infection.

Our unexpected observation was the downregulation of the key virulence gene, *tdh* (2.16-fold, *p*-adj=0.02, **Fig. 3f**) in the mutants, suggesting that they might have reduced virulence. Accordingly, we compared the lethality of wildtype and Δ*puuA*/Δ*puuC* mutant strains in mice following intraperitoneal infection. Consistent with *tdh* downregulation, both mutants exhibited reduced lethality, with Δ*puuA* showing a significantly reduced lethality (**Fig. 3j**). These findings together revealed the impact of Puu-gene-loss on phenotypes related to human infection, including cell adhesion, intestinal colonization and virulence.

Phenotypes of wave-4 strains

To link the phenotypes related to Puu-gene-loss observed in mutant strains with the behavior of natural strains, we next compared 12 natural strains for similar phenotypes as described above, including six wave-1 to wave-3 (2 strains each) and six wave-4 strains (**Fig. 4a**). Consistent with the established phenotypic differences between wildtype and mutant strains, the wave-4 strains exhibited decreased growth when putrescine was used as sole carbon or nitrogen source, with enhanced biofilms and cell adhesion compared with wave-1 to wave-3 strains (**Fig. 4a-c**). Additionally, we analyzed the clinical symptom data of 1,966 PC-related patients reported in our previous study[21], and found that wave-4 was associated with milder symptoms, including significantly lower rates of fever, vomiting and abdominal pain (**Fig. 4d**), consistent with our mouse infection experiment.

We hypothesize that these phenotypic differences mediated by Puu-gene-loss might confer competitive advantages. Therefore, we performed competition experiments for natural strains in seawater with chitin as a nutrition source, mimicking the possible natural environment. We mixed wave-4 strains with those from other waves in equal (1:1) or different (1:5) ratios. By targeted PCR amplification of a gene with a wave-4-specific SNP allele (VPA0427 A919G), we quantified the relative abundance of wave-4 based on the frequency of wave-4-specific allele. After 72 hours of competition, we measured a significant increase in the frequency of wave-4-specific alleles for both mixing ratios (**Fig. 4e**), demonstrating the competition advantage of wave-4 under the tested condition.

Puu-gene-loss in bacteria

Puu-gene-loss could be attributed to selection or genetic drift. Convergent Puu-gene-loss and/or its fixation in specific lineages would provide evidence supporting the selection hypothesis. We analyzed the prevalence of Puu-genes among 108,526 genomes from 36 bacterial species, including *Vibrio*, common pathogens, and probiotics. Puu-genes were not conserved among bacteria, with part of the pathway lost in some species (**Fig. 5** and **Extended Data Table 2**). Notably, the absence/pseudogenization of Puu-genes in strains

within species was convergently identified across multiple species (**Fig. 5b** and **Extended Data Fig. 10**). Furthermore, this absence/pseudogenization was fixed or nearly fixed in a specific lineage for species such as *E. coli*, *Shigella boydii*, *S. sonnei* and *P. aeruginosa*, or convergently occurred in two or more lineages among species such as *Campylobacter coli*, *Yersinia pestis*, *Bifidobacterium longum* and *Lactobacillus helveticus*. Additionally, Puu-gene-loss was not only identified among *V. parahaemolyticus* PC strains, but also identified in the *V. cholerae* 7PET **(Fig. 5b)**.

To test if Puu-gene-loss has a similar phenotypic effect in other bacteria, we generated deletion strains in *V. cholerae* (Δ*puuA* and Δ*spuC*, E7946 background) and *E. coli* (Δ*puuA* and Δ*puuC*, MG1655 background) and tested their biofilm formation and cell adhesion abilities. Consistent with the results in *V. parahaemolyticus*, the mutants generally exhibited significantly enhanced biofilms and adhesion compared to wildtypes, and adding exogenous putrescine further enhanced biofilms (**Fig. 5b**). Together, these results indicate that the Puu-gene-loss is likely under selection and mediated phenotypic changes likely universal across bacterial species.

Discussion

Leveraging a large-scale genome dataset of global isolates, we present the most comprehensive genomic view on the origin and evolution of *V. parahaemolyticus* PC. Our findings suggest that PC likely originated from a serotype O3:K6 pathogenic strain through explosive gain of multiple genes/islands from *V. parahaemolyticus*, rather than from non-pathogenic strains or other *Vibrio* species[11]. Notably, several characteristics previously considered to be specific to PC[10–12], including ST3, *toxRS*/new, and VPaI-1 to VPaI-3, were also present in pre-PC strains, while *orf8* gene remained unique to PC, thus remaining as a reliable maker. Moreover, we described the fine-scale population structure and spatiotemporal dynamics of PC, and identified 'wave succession' with underlying molecular mechanisms. Together, our findings substantially enhance the current understanding of how epidemic lineages of *V. parahaemolyticus* emerge and evolve.

During the evolution of *V. parahaemolyticus* PC, we observed intriguing parallels with *V. cholerae* 7PET and other pathogens. First, we observed explosive gain of genes/islands, including key virulence genes (*tdh* and *ctxAB*) and marker genomic islands (six VPaIs and two VSPs) for *V. parahaemolyticus* PC and *V. cholerae* 7PET. This phenomenon was also observed during human colonization by other pathogens[22] and in the evolution of metabolic pathways across prokaryotic lineages[23]. Frequent human-mediated cross-regional transmission and adaptation to new environments are considered potential drivers for *V. cholerae* 7PET[4], which might also apply to *V. parahaemolyticus* PC. Second, for both PCs from pandemic *Vibrio* species, the inferred times of origin (1983 and 1955[4]) and introduction to specific geographical regions (e.g. South America: 1990 and 1989[24]) were much earlier than their first epidemiological observations (1995 and 1961; South America: 1997 and 1991). Two possible explanations for this include variability in the molecular clock rate[25] with higher early mutation rates[26,27], and the possibility of early cryptic disease epidemics, with specific events such as El Niño or warming in coastal conditions triggering a sudden surge in cases

and thereby drawing epidemiological attention. While the second explanation does not apply to *V. cholerae* due to the high risk and strict surveillance of cholera, both explanations are applicable to *V. parahaemolyticus*. Third, divergence into successive sublineages mediating waves of infections, identified in both pandemic *Vibrio* and other pathogens such as SARS-Cov-2[28]. While antimicrobial resistance likely drove the wave succession of *V. cholerae* 7PET[7], *V. parahaemolyticus* exhibits low resistance rates to first-line antibiotics, indicating a different driving factor.

The importance of biofilm formation in bacterial environmental adaptation and survival under adverse conditions (e.g. antibiotic exposure) is well recognized[29]. Therefore, the enhanced biofilms medicated by Puu-gene-loss likely improve strain's environmental adaptability, as suggested by our competition experiment results. Furthermore, human activities are pivotal in pathogen transmission. Puu-gene-loss not only increases cell adhesion and intestinal colonization, directly facilitating human-mediated transmissions, but also reduces virulence and is associated with milder clinical symptoms, thereby reducing the likelihood of seeking medical attention and promoting cryptic transmissions. Thus, *V. parahaemolyticus* wave succession is likely driven by the fitness advantages of environmental adaptation and human-mediated transmission conferred by Puu-gene-loss. However, every coin has two sides. Puu-gene-loss also brings disadvantages, such as the decreased growth when putrescine sever as the sole nutrient source.

The effects of Puu-genes on biofilm and the underlying mechanisms are likely universal among bacteria. We have demonstrated that Puu-gene-loss or exogenous putrescine enhances biofilms in three different species. Furthermore, Puu-gene-loss in *P. aeruginosa* also leads to enhanced biofilms[19], and *E. coli* phylogroup B2, characterized by absence of *puuA-D* (**Fig. 5b**) exhibits a stronger biofilm-formation ability than other phylogroups[30,31], providing further evidence for a universal effect. Additionally, we propose that the increased extracellular putrescine caused by Puu-gene-loss enhances biofilms by upregulating biofilm and biofilm-related genes, as well as promoting c-di-GMP synthesis. This effect of putrescine on c-di-GMP synthesis was also reported in *P. aeruginosa*[19], suggesting a universal mechanism.

For the first time, we have established links between Puu-gene-loss, cell adhesion and intestinal colonization, which are also likely universal across bacteria. We demonstrate that Puu-gene-loss enhances cell adhesion in three different species and promotes intestinal colonization in *V. parahaemolyticus*. Furthermore, *E. coli* phylogroup B2 are often associated with urinary tract infections[32] and has shown increased persistence in the intestines of human infants[33], both of which is consistent with the hypothesis of increased adhesion and colonization mediated by Puu-gene-loss. Interestingly, the probiotic *E. coli* strain Nissle 1917, known for its strong capability of human gut colonization[34], belongs to phylogroup B2 and lacks Puu-genes (**Fig. 5b**). The upregulation of CupE-fimbriae and Flp-pili genes induced by increased extracellular putrescine may be related to the enhanced cell adhesions, but the underlying molecular mechanism requires further exploration.

The convergent loss or pseudogenization of Puu-gene within species (e.g. *C. coli*) and across

different bacterial species, along with its lineage-specific fixation (e.g. *E. coli*), indicate that these events are more likely selection-driven and may confer fitness advantages. Puu-gene loss/pseudogenization was uniquely fixed in major pathogenic clonal complexes (CC) of *S. boydii* (CC145) and *S. sonnei* (CC152)[35], and recently fixed in *V. parahaemolyticus* wave-4, suggesting potential fitness advantages for human infection or transmission. However, this appears to not always the case, as Puu-gene loss/pseudogenization has not occurred in major pathogenic lineages of *C. coli* and *P. aeruginosa*. Additionally, Puu-gene loss/pseudogenization appears to be associated with lineage divergence in *E. coli* and *C. coli*, and Puu-gene gain is potentially linked to human adaptation in probiotic *B. longum*, with Puu-genes predominantly identified in adult human strains and absent in infant or non-human strains. These observations together indicate that while Puu-gene loss/pseudogenization is likely selection-driven, the underlying driving forces vary across different species.

While the significance of spontaneous mutation and gene acquisition in pathogen evolution is well recognized[36–38], the role of gene loss remains underexplored. Gene loss is pervasive across all life kingdoms[39]. In bacteria, it is commonly found in symbionts and host-dependent pathogens, generally considered neutral and driven by genetic drift associated with transmission bottleneck[40,41], while certain specific genes were experimentally validated to be associated with pathogen virulence[42,43]. Free-living bacteria are better models for investigating gene-loss-driven adaptative evolution due to their large effective population sizes, with gene-loss fixation being expected to be adaptative and selection-driven. Some free-living bacteria, such as the abundant open-ocean bacterioplankton *Prochlorococcus*, exhibit extensive gene loss, which has been attributed to accelerated evolution and fitness advantages conferred by genomic and metabolic "streamlining"[44,45]. Moreover, previously studies of gene loss-mediated bacterial adaptation, whether for symbionts, host-dependent pathogens, or free-living species, generally come with the cost of transition from generalists capable of surviving in diverse environments to specialists adapted to specific ecological niches[42–45]. The exact niche of *V. parahaemolyticus* PC remains unclear but it is more likely a generalist due to widespread distribution in marine and aquatic habitats. If we consider different geographical regions as the macro-niches, the wave-4 characterized by Puu-gene-loss has spread globally, without clear evidence supporting its transition from generalists to specialists. Additionally, to the best of our knowledge, there are no reports of gene loss-mediated adaptation in free-living pathogens. Therefore, our study presents a novel paradigm of pathogen adaptation by gene loss.

In summary, our study provides the most comprehensive genomic view on the origin and evolution of *V. parahaemolyticus* PC. We identified several interesting common features between two pandemic *Vibrio* species, but the driving forces underlying wave succession events appear distinct. While spontaneous mutation and gene gain-mediated antibiotic resistance may drive the *V. cholerae* 7PET succession[7], we demonstrated that Puu-gene loss, which confers phenotypic advantages related to environmental adaptation and human transmission, has likely driven the recent *V. parahaemolyticus* wave succession. An interesting finding is that *V. parahaemolyticus* wave succession has come along with reduced virulence and possibly increased transmission rates, which aligns with the trade-off

hypothesis of pathogen virulence evolution[46]. We also found that Puu-gene-loss is general and frequent among bacteria, selection-driven, with its phenotypic impacts and underly mechanisms likely universal across species. Furthermore, Puu-gene-loss may play key roles in bacterial evolution, including lineage divergence (e.g. *E. coli*, *C. coli* and *B. longum*), human adaptation (e.g. *B. longum*) and the epidemic expansion of specific pathogenic lineages (e.g. *V. parahaemolyticus*, *S. boydii* and *S. sonnei*). Taken together, our findings provide a novel paradigm of adaptative evolution by gene loss in a pandemic pathogen.

Methods

V. parahaemolyticus genome dataset

A total of 8,684 high-quality genomes were included in this study, including 333 newly sequenced and 8,351 publicly available genomes (**Supplementary Table 1**). Public genomes (up to November 2022) were downloaded from National Center for Biotechnology Information GenBank or Sequence Read Archive (SRA) database, with metadata extracted from corresponding BioSample information or the literatures. New genomes were obtained from archived strains isolated from multiple countries, including China, Japan, Senegal, Peru and Chile.

Whole genome sequencing of new strains was performed using Illumina NovaSeq or Miseq platforms. New and public sequencing reads were trimmed using Trimmomatic v0.39[47] and were *de novo* assembled using shovill v1.1.0 pipeline (https://github.com/tseemann/shovill). The quality assessment of genomes was performed using CheckM v1.1.3[48]. Whole genome average nucleotide identity (ANI) against the reference genome of *V. parahaemolyticus* (RIMD2210633, accession numbers: NC_004603.1 and NC_004605.1) was calculated using fastANI v1.1[49]. Only high-quality genomes (completeness >90% or contamination <5%) with ANI >95% were included in further analysis.

Phylogenetic analysis

Genome sequences were aligned against the reference genome using MUMmer v3.23[50] to generate whole-genome alignments. Core-genome (regions present in >99% strains) single-nucleotide polymorphisms (SNPs) were identified using SNP-sites v2.5.1[51]. SNPs located in repetitive regions identified by TRF v4.07b[52] or BLASTN self-search were excluded. Non-repetitive SNPs were used to construct maximum-likelihood phylogenetic trees using FastTree v2.1.10[53] or RAxML-NG v1.0.1[54]. Recombination regions were detected using Gubbins v3.1.3[55]. Homoplastic SNPs were identified using SNPPar v1.0[56]. Recombined and homoplastic SNPs were excluded from the phylogenetic analysis of pandemic clone (PC) and pre-PC isolates. Phylogenetic trees were visualized using ggtree[57]. Hierarchical clustering analysis were performed using fastBAPS v1.0.6[58] to assign strains into subgroups.

Serotype and MLST typing

In silico O- and K-antigen genotyping was performed using *V. parahaemolyticus* Kaptive database[59]. Multi-locus sequence typing (MLST) was performed using mlst (https://github.com/tseemann/mlst) to scan genome sequences against the PubMLST databases.

Representative genome dataset of PC

We generated a representative subset of 942 PC isolates. First, to reduce the effect of repeat sampling such as strains from disease outbreaks, we selected the genome with maximum N50 from a cluster of strains with ≤6 SNPs from same country and within a year, representing putative outbreaks[21]. Second, we calculated root-to-tip distances of phylogenetic trees based on non-recombined SNPs, and removed putative hypermutators with extreme root-to-tip distances and branch lengths (**Extended Data Fig. 3**).

Temporal analysis and population size dynamics

Temporal signals were investigated using TempEst v1.5.3[60] by calculating the correlation between root-to-tip distances and isolation dates (years). For strains with significant temporal signals (p<0.05), we re-constructed phylogenetic trees and applied BactDating v1.1.0[61] to infer the dated phylogenetic trees. Effective population size dynamics was inferred using skygrowth v0.3.1[62] based on dated trees.

Core-pangenome

All PC representative genomes were re-annotated using Prokka v1.13[63], and the annotation outputs (GFF3 files) were used in Panaroo v1.2.8[64] to identify the core-pangenome and gene presence/absence.

Wave-4 specific variations

We analyzed three types of variations, including SNPs, gene presence/absence and unitigs. The SNPs and gene presence/absence data were extracted from the preceding analysis. The unitig matrix was determined using unitig-caller v1.2.1 (https://github.com/bacpop/unitig-caller). Unitig sequences were aligned against assembled genomes using BLASTN to identify corresponding genomic positions and related genes. Wave-4 specific variations were defined as alleles, genes or unitigs present/absent in >95% of wave-4 strains and <5% of non-wave-4 strains.

Puu-genes in bacteria

We investigated the prevalence of Puu-genes in 36 bacterial species, including *Vibrio*, common pathogens, and probiotics. We included a total of 108,526 genomes (62-24,205 genomes per species, **Supplementary Table 6**) downloaded from Genome Taxonomy Database (GTDB, release207)[65]. Puu-related protein sequences in *E. coli*, *P. aeruginosa* and *V. parahaemolyticus* were used as initial queries, which were searched against all genomes of the selected 36 species using TBLASTN to identify the reference genes of each species (**Extended Data Table 2**). Nucleotide and protein sequences of the reference genes for each species were then searched against all genomes of the corresponding species using BLASTN and TBLASTN. We combined BLASTN and TBLASTN results to identify the presence, absence or pseudogenization of genes, with identify >80% and coverage >70% as cutoffs. A gene was classified as present if a BLASTN or TBLASTN match was identified. If only a BLASTN match was identified, the gene was classified as a pseudogene; otherwise, it was considered absent.

Bacterial strains and growth conditions

A total of 12 *V. parahaemolyticus* representative strains (pairwise SNP distances: >6) were used for laboratory experiments, including reference strain RIMD2210633 (wave-3) and 11 previously or newly sequenced PC strains. Additionally, *V. cholerae* strain E7946 (El Tor, Ogawa) and *E. coli* strain MG1655 (K12) were included. *V. parahaemolyticus* strains were grown routinely in rich broth (LB with 3% NaCl) with shaking or on agar plates at 30°C aerobically. *E. coli* and *V. cholerae* strains were cultured in LB at 37°C.

Mutant construction

Deletion mutants of *V. parahaemolyticus* (Δ*puuA* and Δ*puuC*) were constructed by homologous recombination and counterselection with the suicide plasmid pDM4 as previously described[66], with 1kb of homology upstream and downstream of the desired mutation. For *V. cholerae*, a similar approach with pDM4 was used as for *V. parahaemolyticus* (Δ*puuC* and Δ*spuC*), except *E. coli* MFD*pir* was used as donor strain for conjugation. *E. coli* deletion mutants (Δ*puuA* and Δ*puuC*) were constructed using λ red recombination as previously described[67]. *V. parahaemolyticus* deletion strains were complemented with the corresponding gene *in trans* on plasmid pMMB207 using the Ptac promoter. All deletion and complement clones were verified by colony PCR. All constructed strains and plasmids are listed in **Supplementary Table 7**.

Growth curves

The growth of strains was tested under three conditions: rich/high-salt medium (alkaline peptone water [APW] with 3% NaCl, Beijing Land Bridge technology), modified M9-Put-As medium (putrescine as sole carbon source, M9 medium supplemented with 0.04 M Na_2HPO_4, 0.02 M KH_2PO_4,0.42 mM $MgSO_4$, 1mM $CaCl_2$, 3% NaCl, 0.4% $(NH4)_2SO_4$, 0.4% putrescine dihydrochloride, Sangon Biotech) and modified W-Glc-Put medium (putrescine as the sole nitrogen source, M9 medium supplemented with 0.06 M K_2HPO4, 0.03 M KH_2PO_4, 0.42 mM $MgSO_4$, 1mM $CaCl_2$, 3% NaCl, 0.4% glucose, 0.2% putrescine dihydrochloride)[18].

All *V. parahaemolyticus* strains were initially cultured overnight in APW with 3% NaCl at 37°C, followed by 1:100 dilution and growth to logarithmic phase. Log-phage cultures were inoculated into specified media and monitored for growth rate every 15 min at OD_{600} for 24 or 72 hours at 37°C under static conditions using BioTek Synergy H1 (Agilent Technologies).

Biofilm assays

Log-phase cultures were inoculated into different media (APW or M9 with 3% NaCl, or M9 with 1% NaCl) in 96-well plates (Kingmorn biotechnology) and incubated under static conditions at 37°C for 48 hours. Following incubation, culture media was discarded, and 96-well plates were washed with 0.9% NaCl twice, dried at 60 °C for 30 min, and stained with 100 μl 0.1% (w/v) crystal violet solution for 10 min. After staining, the plates were washed with 0.9% NaCl three times. The bound crystal violet was resolubilized with 100 μl 95% ethanol for 10 min and quantified via OD_{595} with BioTek Synergy H1 (Agilent Technologies). Each strain was tested with 30 technical replicates.

RNA extraction and transcriptome analysis

Strains were grown to stationary phase in M9 media with 1% NaCl, with or without exogenous putrescine (2.5 mM putrescine dihydrochloride) and harvested after treatment with stop mix (5% phenol, 95% ethanol). Total RNA was extracted from cells using the hot-phenol method as described previously[68]. RNA was DNase I-digested and rRNA depleted. cDNA libraries were constructed at Novogene Co. Ltd. (Beijing, China) and sequenced on an Illumina NovaSeq platform.

Sequencing reads were trimmed using Trimmomatic v0.39[47] and then mapped to the reference genome using BWA v0.7.17[69]. The number of reads assigned to genes were counted using featureCounts v2.0.6[70]. Differentially expressed genes and pathway enrichment analysis were performed using R packages DESeq2 v1.34.0[71] and ClusterProfiler v4.2.2[72].

Metabolite quantification

The OD_{600} of cultures was monitored until the desired growth phases (log-phase: ~4h, stationary phase: ~13h) at 37°C in M9 medium with 1% NaCl. 10 OD_{600} of culture was collected and metabolites were extracted using 100% methanol. Targeted metabolomics to quantify putrescine, GABA and spermidine levels was performed using a Liquid Chromatograph Mass Spectrometer (LC-MS, Thermo Fisher Scientific Inc.) by the Mass Spectrometry services platform at the Shanghai Institute of Immunity and Infection.

c-di-GMP assay

To measure intracellular c-di-GMP, we used a previously published riboswitch-based reporter system[73]. Log-phase cultures of strains carrying the reporter were inoculated into M9 medium with 1% NaCl and 50 µg/ml spectinomycin in 96-well plates (six replicate wells per strain). Additionally, six wells of blank control with 200 µl uninoculated medium were included. The plate was incubated in a BioTek Synergy H1 plate reader (Agilent Technologies) at 37°C for 48 hours. OD_{600} and fluorescence (455 nm excitation/489 nm emission for AmCyan and 540 nm excitation/574 nm emission for TurboRFP) were measured every 15 min. The average values of the control wells were subtracted from each measurement (OD_{600}, AmCyan, and TurboRFP) of the strains. The mean values were used to plot growth curves and the whisker length represents standard deviation.

Cell adhesion

Log-phage strain cultures were washed with PBS and then resuspended in cell culture medium without antibiotics. Caco-2 cells grown in 24-well plates were infected with the bacterial suspension at an MOI of 10:1. After 45 min, cells were washed three times with PBS to remove the non-attached bacteria and then lysed with 0.1% saponin for 10 min. The number of cell-associated bacteria was determined by plating serial dilutions of the lysate on LB agar plates. The percentage of cell-associated bacteria was calculated as (recovered CFU/inoculated CFU) × 100%, and the results were presented as adhesion relative to wild-type strain (RIMD-W3).

Mouse colonization

Female BALB/c mice aged 6-8 weeks were used to test strain colonization. Mice were randomly divided into four groups, including a control group and three groups inoculated with different strains (three mice each treated group). All mice were fasted for 8 hours prior to gavage.

We introduced plasmids with *lux* reporters (pWHQ205, encoding luciferase and substrate, constructed in this study) into three strains (RIMD-W3, Δ*puuA* and Δ*puuC*), respectively. Strains carrying *lux* reporters were cultured in LB medium with 3% NaCl supplemented with chloramphenicol (25 μg/ml) to logarithmic phase (OD_{600}=0.6~0.8) at 30°C. Strain concentration was then adjusted to 3×10^{10} CFU/ml with PBS, and each mouse was gavaged with 0.3 ml of the bacterial suspension. At 5 and 10 hours post-infection, the mice were anesthetized with 3% isoflurane for 5 minutes and exposed for 1 minute using the PerkinElmer IVIS Spectrum imaging system (E-Heng Import and Export Co. Ltd).

Mouse lethality

Female BALB/c mice aged 4-5 weeks were used for lethality experiment, which were randomly divided into five groups treated by different strains, with each consisting of 10 mice. Log-phage strain cultures were washed three times with PBS and then adjusted to a concentration of 10^9 CFU/ml with PBS. Mice were intraperitoneally injected with 100 μl of strain suspension, and the number of mice that died at a specific time point was record. The experimental protocols of colonization and lethality of mice were approved by the animal ethics committee of Shanghai Institute of Immunity and Infection (No. A2023011).

Growth competition assay

Log-phage cultures of 12 natural strains, including six wave-1/2/3 and six wave-4 strains (**Supplementary Table 7**), were individually diluted to an OD_{600} of 0.08. Subsequently, the diluted cultures of wave-4 strains were mixed with those of wave-1 to wave-3 strains in equal (1:1) or different (1:5) ratios. These mixtures were then incubated in seawater (collected from Jinshan, Shanghai) supplemented with 0.5% chitin (Sigma) for 72 hours at 30°C under static conditions. Genomic DNA of harvested cultures was extracted using the TIANamp Bacteria DNA kit (Tiangen Biotech). PCR primers VPA0427SNPU (AGCGACGACGCCAGAGAAAG) and VPA0427SNPD (GGTGTCTAAAGTACGGTGCAG) were used to amplify the gene VPA0427, which contains a wave-4 specific SNP allele (A919G).

The PCR amplification products were used for library construction at Novogene Co. Ltd. (Beijing, China) and sequenced on an Illumina NovaSeq platform. Sequencing reads are trimmed using Trimmomatic v0.39[47] and were then mapped to *V. parahaemolyticus* reference genome using BWA v0.7.17[69]. The frequency of the wave-4 specific allele was calculated to represent the relative abundance of wave-4 strains.

Data availability

The sequencing data have been deposited in the NCBI SRA or GenBank database under

accession number PRJNA1117214 and PRJNA1062747. Background information of sequenced isolate is listed in Supplementary Table 1-2. Source data are provided with this paper.

Reference

1. Bonneaud, C. & Longdon, B. Emerging pathogen evolution: Using evolutionary theory to understand the fate of novel infectious pathogens. *EMBO Rep* **21**, (2020).
2. Balasubramanian, D., López-Pérez, M., Grant, T. A., Ogbunugafor, C. B. & Almagro-Moreno, S. Molecular mechanisms and drivers of pathogen emergence. *Trends in Microbiology* vol. 30 (2022).
3. Baker-Austin, C. *et al.* Vibrio spp. infections. *Nat Rev Dis Primers* **4**, 8 (2018).
4. Hu, D. *et al.* Origins of the current seventh cholera pandemic. *Proc Natl Acad Sci U S A* **113**, E7730–E7739 (2016).
5. Mutreja, A. *et al.* Evidence for several waves of global transmission in the seventh cholera pandemic. *Nature* **477**, 462–465 (2011).
6. Didelot, X. *et al.* The Role of China in the Global Spread of the Current Cholera Pandemic. *PLoS Genet* **11**, (2015).
7. Weill, F.-X. *et al.* Genomic History of the Seventh Pandemic of Cholera in Africa. *Science*, **358**: 785-789 (2017).
8. Baker-Austin, C., Stockley, L., Rangdale, R. & Martinez-Urtaza, J. Environmental occurrence and clinical impact of Vibrio vulnificus and Vibrio parahaemolyticus: A European perspective. *Environ Microbiol Rep* **2**, 7–18 (2010).
9. Yang, C. *et al.* Recent mixing of Vibrio parahaemolyticus populations. *ISME J* **13**, 2578–2588 (2019).
10. Nair, G. B. *et al.* Global dissemination of Vibrio parahaemolyticus serotype O3:K6 and its serovariants. *Clin Microbiol Rev* **20**, 39–48 (2007).
11. Espejo, R. T., García, K. & Plaza, N. Insight into the origin and evolution of the Vibrio parahaemolyticus pandemic strain. *Front Microbiol* **8**, 1–6 (2017).
12. Han, D., Yu, F., Chen, X., Zhang, R. & Li, J. Challenges in Vibrio parahaemolyticus infections caused by the pandemic clone. *Future Microbiol* **14**, 437–450 (2019).
13. Matsumoto, C. *et al.* Pandemic spread of an O3:K6 clone of Vibrio parahaemolyticus and emergence of related strains evidenced by arbitrarily primed PCR and toxRS sequence analyses. *J Clin Microbiol* **38**, (2000).
14. Nasu, H. *et al.* A filamentous phage associated with recent pandemic Vibrio parahaemolyticus O3:K6 strains. *J Clin Microbiol* **38**, (2000).
15. Hurley, C. C., Quirke, A. M., Reen, F. J. & Boyd, E. F. Four genomic islands that mark post-1995 pandemic Vibrio parahaemolyticus isolates. *BMC Genomics* **7**, 1–19 (2006).
16. Boyd, E. F. *et al.* Molecular analysis of the emergence of pandemic Vibrio parahaemolyticus. *BMC Microbiol* **8**, 1–14 (2008).
17. Cui, Y. *et al.* Epidemic clones, oceanic gene pools, and eco-LD in the free living marine pathogen vibrio parahaemolyticus. *Mol Biol Evol* **32**, 1396–1410 (2015).
18. Schneider, B. L. & Reitzer, L. Pathway and enzyme redundancy in putrescine catabolism in Escherichia coli. *J Bacteriol* **194**, (2012).
19. Liu, Z., Hossain, S. S., Moreira, Z. M. & Haney, C. H. Putrescine and Its Metabolic

Precursor Arginine Promote Biofilm and c-di-GMP Synthesis in Pseudomonas aeruginosa. *J Bacteriol* **204**, (2022).

20. Kline, K. A., Fälker, S., Dahlberg, S., Normark, S. & Henriques-Normark, B. Bacterial Adhesins in Host-Microbe Interactions. *Cell Host and Microbe* **5**, (2009).
21. Yang, C. *et al.* Outbreak dynamics of foodborne pathogen Vibrio parahaemolyticus over a seventeen year period implies hidden reservoirs. *Nat Microbiol* **7**, 1221–1229 (2022).
22. Datta, M. S. *et al.* Rapid methicillin resistance diversification in Staphylococcus epidermidis colonizing human neonates. *Nat Commun* **12**, (2021).
23. Iwasaki, W. & Takagi, T. Rapid pathway evolution facilitated by horizontal gene transfers across prokaryotic lineages. *PLoS Genet* **5**, (2009).
24. Domman, D. *et al.* Integrated View of *Vibrio Cholerae* in the Americas. *Science*, **358**, 789-793 (2017).
25. Cui, Y. *et al.* Historical variations in mutation rate in an epidemic pathogen, Yersinia pestis. *Proceedings of the National Academy of Sciences* **110**, 577–582 (2013).
26. Rabosky, D. L. & Lovette, I. J. Explosive evolutionary radiations: Decreasing speciation or increasing extinction through time? *Evolution* **62**, (2008).
27. Morlon, H., Kemps, B. D., Plotkin, J. B. & Brisson, D. Explosive radiation of a bacterial species group. *Evolution* **66**, (2012).
28. Markov, P. V. *et al.* The evolution of SARS-CoV-2. *Nature Reviews Microbiology* **21**, (2023).
29. Flemming, H. C. *et al.* Biofilms: An emergent form of bacterial life. *Nature Reviews Microbiology* **14**, (2016).
30. Wang, Y. *et al.* Isolation, phylogenetic group, drug resistance, biofilm formation, and adherence genes of Escherichia coli from poultry in central China. *Poult Sci* **95**, (2016).
31. Flament-Simon, S. C. *et al.* Association between kinetics of early biofilm formation and clonal lineage in Escherichia coli. *Front Microbiol* **10**, (2019).
32. Hogins, J., Xuan, Z., Zimmern, P. E. & Reitzer, L. The distinct transcriptome of virulence-associated phylogenetic group B2 Escherichia coli . *Microbiol Spectr* **11**, (2023).
33. Nowrouzian, F. L., Wold, A. E. & Adlerberth, I. Escherichia coli strains belonging to phylogenetic group B2 have superior capacity to persist in the intestinal microflora of infants. *Journal of Infectious Diseases* **191**, (2005).
34. Grozdanov, L. *et al.* Analysis of the genome structure of the nonpathogenic probiotic Escherichia coli strain Nissle 1917. *J Bacteriol* **186**, (2004).
35. Chattaway, M. A., Schaefer, U., Tewolde, R., Dallman, T. J. & Jenkins, C. Identification of Escherichia coli and shigella species from whole-genome sequences. *J Clin Microbiol* **55**, (2017).
36. Viana, D. *et al.* A single natural nucleotide mutation alters bacterial pathogen host tropism. *Nat Genet* **47**, (2015).
37. Arnold, B. J., Huang, I. T. & Hanage, W. P. Horizontal gene transfer and adaptive evolution in bacteria. *Nature Reviews Microbiology* **20**, 206–218 (2022).
38. Rodríguez-Beltrán, J., DelaFuente, J., León-Sampedro, R., MacLean, R. C. & San Millán, Á. Beyond horizontal gene transfer: the role of plasmids in bacterial evolution. *Nature Reviews Microbiology* **19**, 347–359 (2021).
39. Albalat, R. & Cañestro, C. Evolution by gene loss. *Nature Reviews Genetics* **17**, 379–391

(2016).
40. Pallen, M. J. & Wren, B. W. Bacterial pathogenomics. *Nature* **449**, 835–842 (2007).
41. McCutcheon, J. P. & Moran, N. A. Extreme genome reduction in symbiotic bacteria. *Nature Reviews Microbiology* **10**, 13–26 (2012).
42. Maurelli, A. T. Black holes, antivirulence genes, and gene inactivation in the evolution of bacterial pathogens. *FEMS Microbiology Letters* **267**, (2007).
43. Bliven, K. A. & Maurelli, A. T. Antivirulence genes: Insights into pathogen evolution through gene loss. *Infection and Immunity* **80**, 4061–4070 (2012).
44. Dufresne, A., Garczarek, L. & Partensky, F. Accelerated evolution associated with genome reduction in a free-living prokaryote. *Genome Biol* **6**, (2005).
45. Morris, J. J., Lenski, R. E. & Zinser, E. R. The black queen hypothesis: Evolution of dependencies through adaptive gene loss. *mBio* **3**, (2012).
46. Alizon, S., Hurford, A., Mideo, N. & Van Baalen, M. Virulence evolution and the trade-off hypothesis: History, current state of affairs and the future. *Journal of Evolutionary Biology* **22**, (2009).
47. Bolger, A. M., Lohse, M. & Usadel, B. Trimmomatic: a flexible trimmer for Illumina sequence data. *Bioinformatics* **30**, 2114–2120 (2014).
48. Parks, D. H., Imelfort, M., Skennerton, C. T., Hugenholtz, P. & Tyson, G. W. CheckM: Assessing the quality of microbial genomes recovered from isolates, single cells, and metagenomes. *Genome Res* **25**, 1043–1055 (2015).
49. Jain, C., Rodriguez-R, L. M., Phillippy, A. M., Konstantinidis, K. T. & Aluru, S. High throughput ANI analysis of 90K prokaryotic genomes reveals clear species boundaries. *Nat Commun* **9**, 1–8 (2018).
50. Delcher, A. L., Salzberg, S. L. & Phillippy, A. M. Using MUMmer to Identify Similar Regions in Large Sequence Sets . *Curr Protoc Bioinformatics* **00**, (2003).
51. Page, A. J. *et al.* SNP-sites: rapid efficient extraction of SNPs from multi-FASTA alignments. *Microb Genom* **2**, e000056 (2016).
52. Benson, G. Tandem repeats finder: a program to analyze DNA sequences. *Nucleic Acids Res* **27**, 573–580 (1999).
53. Price, M. N., Dehal, P. S. & Arkin, A. P. FastTree 2 – Approximately Maximum-Likelihood Trees for Large Alignments. *PLoS One* **5**, e9490 (2010).
54. Kozlov, A. M. *et al.* RAxML-NG: A fast, scalable and user-friendly tool for maximum likelihood phylogenetic inference. *Bioinformatics* **35**, 4453-4455 (2019).
55. Croucher, N. J. *et al.* Rapid phylogenetic analysis of large samples of recombinant bacterial whole genome sequences using Gubbins. *Nucleic Acids Res* **43**, e15 (2015).
56. Edwards, D., Duchêne, S., Pope, B. & Holt, K. SNPPar: identifying convergent evolution and other homoplasies from microbial whole-genome alignments. **264017**, 1–33 (2020).
57. Yu, G., Smith, D. K., Zhu, H., Guan, Y. & Lam, T. T. Y. ggtree: an r package for visualization and annotation of phylogenetic trees with their covariates and other associated data. *Methods Ecol Evol* **8**, (2017).
58. Tonkin-Hill, G., Lees, J. A., Bentley, S. D., Frost, S. D. W. & Corander, J. Fast hierarchical Bayesian analysis of population structure. *Nucleic Acids Res* **47**, 5539–5549 (2019).
59. van der Graaf-Van Bloois, L., Chen, H., Wagenaar, J. A. & Zomer, A. L. Development of Kaptive databases for Vibrio parahaemolyticus O-and K-antigen genotyping. *Microb*

Genom **9**, (2023).
60. Rambaut, A., Lam, T. T., Carvalho, L. M. & Pybus, O. G. Exploring the temporal structure of heterochronous sequences using TempEst (formerly Path-O-Gen). *Virus Evol* **2**, (2016).
61. Didelot, X., Croucher, N. J., Bentley, S. D., Harris, S. R. & Wilson, D. J. Bayesian inference of ancestral dates on bacterial phylogenetic trees. *Nucleic Acids Res* **46**, (2018).
62. Volz, E. M. & Didelot, X. Modeling the growth and decline of pathogen effective population size provides insight into epidemic dynamics and drivers of antimicrobial resistance. *Syst Biol* **67**, 719–728 (2018).
63. Seemann, T. Prokka: rapid prokaryotic genome annotation. *Bioinformatics* **30**, 2068–2069 (2014).
64. Tonkin-Hill, G. *et al.* Producing polished prokaryotic pangenomes with the Panaroo pipeline. *Genome Biol* **21**, 180 (2020).
65. Parks, D. H. *et al.* GTDB: An ongoing census of bacterial and archaeal diversity through a phylogenetically consistent, rank normalized and complete genome-based taxonomy. *Nucleic Acids Res* **50**, D785–D794 (2022).
66. Chimalapati, S., Lafrance, A. E., Chen, L. & Orth, K. Vibrio parahaemolyticus: Basic Techniques for Growth, Genetic Manipulation, and Analysis of Virulence Factors. *Curr Protoc Microbiol* **59**, (2020).
67. Datsenko, K. A. & Wanner, B. L. One-step inactivation of chromosomal genes in Escherichia coli K-12 using PCR products. *Proc Natl Acad Sci U S A* **97**, (2000).
68. Sharma, C. M., Darfeuille, F., Plantinga, T. H. & Vogel, J. A small RNA regulates multiple ABC transporter mRNAs by targeting C/A-rich elements inside and upstream of ribosome-binding sites. *Genes Dev* **21**, (2007).
69. Li, H. & Durbin, R. Fast and accurate short read alignment with Burrows-Wheeler transform. *Bioinformatics* **25**, 1754–1760 (2009).
70. Liao, Y., Smyth, G. K. & Shi, W. FeatureCounts: An efficient general purpose program for assigning sequence reads to genomic features. *Bioinformatics* **30**, (2014).
71. Love, M. I., Huber, W. & Anders, S. Moderated estimation of fold change and dispersion for RNA-seq data with DESeq2. *Genome Biol* **15**, (2014).
72. Wu, T. *et al.* clusterProfiler 4.0: A universal enrichment tool for interpreting omics data. *The Innovation* **2**, 100141 (2021).
73. Zhou, H. *et al.* Characterization of a natural triple-tandem c-di-GMP riboswitch and application of the riboswitch-based dual-fluorescence reporter. *Sci Rep* **6**, (2016).

Acknowledgements

This work was supported by National Natural Science Foundation of China (No. 32270003 and No. 32000008 to C.Y., No. 32170640 and No.32211550014 to D.F., No. 32250610209 to S.S.), Youth Innovation Promotion Association, Chinese Academy of Sciences (No. 2022278 to C.Y.), National Key Research and Development Program of China (No. 2022YFC2304700 to F.D.), Shanghai Rising-Star Program (No. 23QA1410500 to C.Y.), Shanghai Public Health System Construction Three-Year Action Plan (No. GWVI-11.1-43 to H.Q.) and Wuxi Science and Technology Development Fund's 'Light of Taihu Lake' Science and Technology Research Program (Basic Research) (No. K20231033 to C.N., No. K20231045 to S.G.). We are grateful to the labs of Prof. Qiyao Wang, Kim Orth, and Jin He for providing strains and plasmids. We thank Prof. Lei Pan for valuable comments.

Author contributions

C.Y., J.M.-U. and D.F. designed, initiated and coordinated the study. J.M.-U., L.X, Y.L., M.J., X.S. and Q.H. contributed to data collection. C.Y., Z.J., J.W., and W.X. performed bioinformatics analysis. H.Q, S.S., C.N., S.G., Z.J., H.W., Y.Q. and S.L. performed experiments. All authors contributed to interpretation of the data. C.Y. wrote the first draft of the paper and H.Q., S.S., Y.Z., Y.C., J.M.-U., H.W., R.Y., Y.C. and D.F. reviewed and revised the paper. All authors read and approved the final manuscript.

Competing interests

The authors declare no competing interests.

Figure legends

Figure 1. From pre-pandemic (pre-PC) to pandemic clone (PC). a) Maximum likelihood tree of 8,684 global isolates. Pre-PC and PC isolates are colored in blue and red, respectively. b) Inferred evolutionary history from pre-PC to PC. The status of known PC marker genes/islands in the ancestral strain is indicated by blue ellipses, while subsequent gains or losses are represented by orange and black triangles. The numbers next to tree nodes indicate inferred divergence times and 95% confidence intervals. c) Distribution of known PC marker genes/islands among pre-PC and PC strains.

Figure 2. Fine-scale population structure, spatiotemporal and population dynamics of PC. a) Maximum likelihood tree of 942 representative PC strains. The colors represent different waves. Double slashes indicate artificially truncated branches. b) Dated phylogeny of PC (left) and the geographical, subtyping and distribution of genes in the putrescine utilization (Puu) pathway of strains (right). The colors of tree branches indicate geographic areas, and numbers next to tree nodes indicate inferred divergence times and 95% confidence intervals. TCs indicate transmissions resulting in local colonization. (c) Temporal dynamics of four waves. Bar colors indicate the frequency of different waves. The line represents the number of representative strains. (d) Temporal distribution of representative strains in different countries and regions. The size of circles scales with the number of representative strains. (e) Effective population size dynamics of different waves of the PC.

Figure 3. Effect of gene-loss in putrescine utilization (Puu) pathway. a) Positions of wave-4 specific variations on the reference genome (top) and gene structure and coverage of Puu-genes (colored in blue) in different waves (bottom). b) Summary of Puu-genes and metabolites based on KEGG annotations. c) Growth curves of wildtype (RIMD-W3), mutants (Δ*puuA* and Δ*puuC*) and complement strains (C-Δ*puuA* and C-Δ*puuC*) when putrescine (Put) was used as sole carbon or nitrogen source. d) Biofilm levels in M9 minimal media with moderate salt concentrations measured by optical density at 595 nm (OD_{595}) with (+Put) or without exogenous putrescine. e) Quantification of intra- and extra-cellular metabolites during logarithmic and stationary phases. N.D.: not detected. f) Transcriptomic volcano plots showing differentially expressed genes (DEGs). The colors represent genes of specific category as in the legend. g) c-di-GMP dynamics of strains with (+Put) or without exogenous putrescine. h) The adhesion ability of strains to Caco-2 cells relative to wildtype (RIMD-W3). i) *In vivo* bioluminescent imaging of mice at 5 hours post-infection by gavage. j) Survival curves of mice by intraperitoneal infection. The measurements in panel e and h were converted into relative level to wildtype. *: $p<0.05$, **: $p<0.01$.

Figure 4. Phenotypes and clinical symptoms of wave1-3 and wave-4 strains. a) Growth curves under high-nutrition and high-salt (APW+ 3%NaCl) conditions and when putrescine was used as the sole carbon or nitrogen source. b) Biofilm level measured by OD_{595} of strains after crystal violet staining. c) The adhesion ability of strains to Caco-2 cells. d) Clinical symptoms of wave-4 and other wave-associated patients. e) Wave-4 specific allele frequency after 72 hours of competition under seawater with chitin conditions.

Figure 5. Puu-genes in 36 bacterial species. a) Prevalence of Puu-genes in 36 species. Genes and sub-pathways (SP) on the left are as in Fig. 3b. The colors (right) indicate the frequency of genes. b) Phylogenetic distribution of Puu-genes in 10 species and the biofilm and adhesion of wildtype (E7946 and MG1655) and mutant strains (Δ*puuA*, Δ*puuC* and Δ*spuC*) in *V. cholerae* and *E. coli* with (+Put) or without exogenous putrescine.

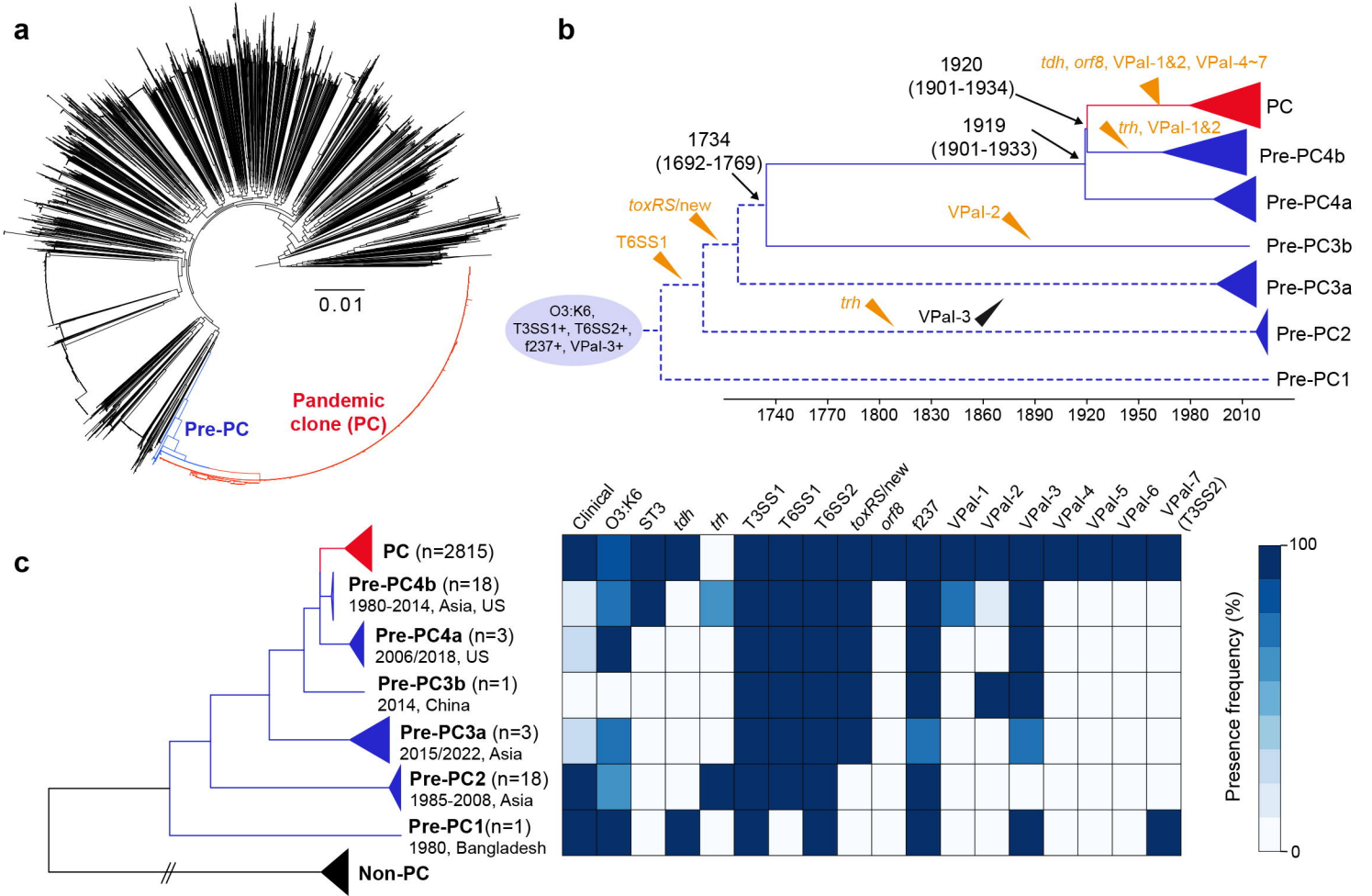
a
0.01
Pre-PC
Pandemic clone (PC)
b
1920 (1901-1934)
tdh, orf8, VPal-1&2, VPal-4~7
PC
1919 (1901-1933)
trh, VPal-1&2
Pre-PC4b
1734 (1692-1769)
Pre-PC4a
toxRS/new
VPal-2
T6SS1
Pre-PC3b
Pre-PC3a
O3:K6, T3SS1+, T6SS2+, f237+, VPal-3+
trh
VPal-3
Pre-PC2
Pre-PC1
1740 1770 1800 1830 1860 1890 1920 1950 1980 2010
c
PC (n=2815)
Pre-PC4b (n=18)
1980-2014, Asia, US
Pre-PC4a (n=3)
2006/2018, US
Pre-PC3b (n=1)
2014, China
Pre-PC3a (n=3)
2015/2022, Asia
Pre-PC2 (n=18)
1985-2008, Asia
Pre-PC1(n=1)
1980, Bangladesh
Non-PC
Clinical
O3:K6
ST3
tdh
trh
T3SS1
T6SS1
T6SS2
toxRS/new
orf8
f237
VPal-1
VPal-2
VPal-3
VPal-4
VPal-5
VPal-6
VPal-7 (T3SS2)
Presence frequency (%)
100
0

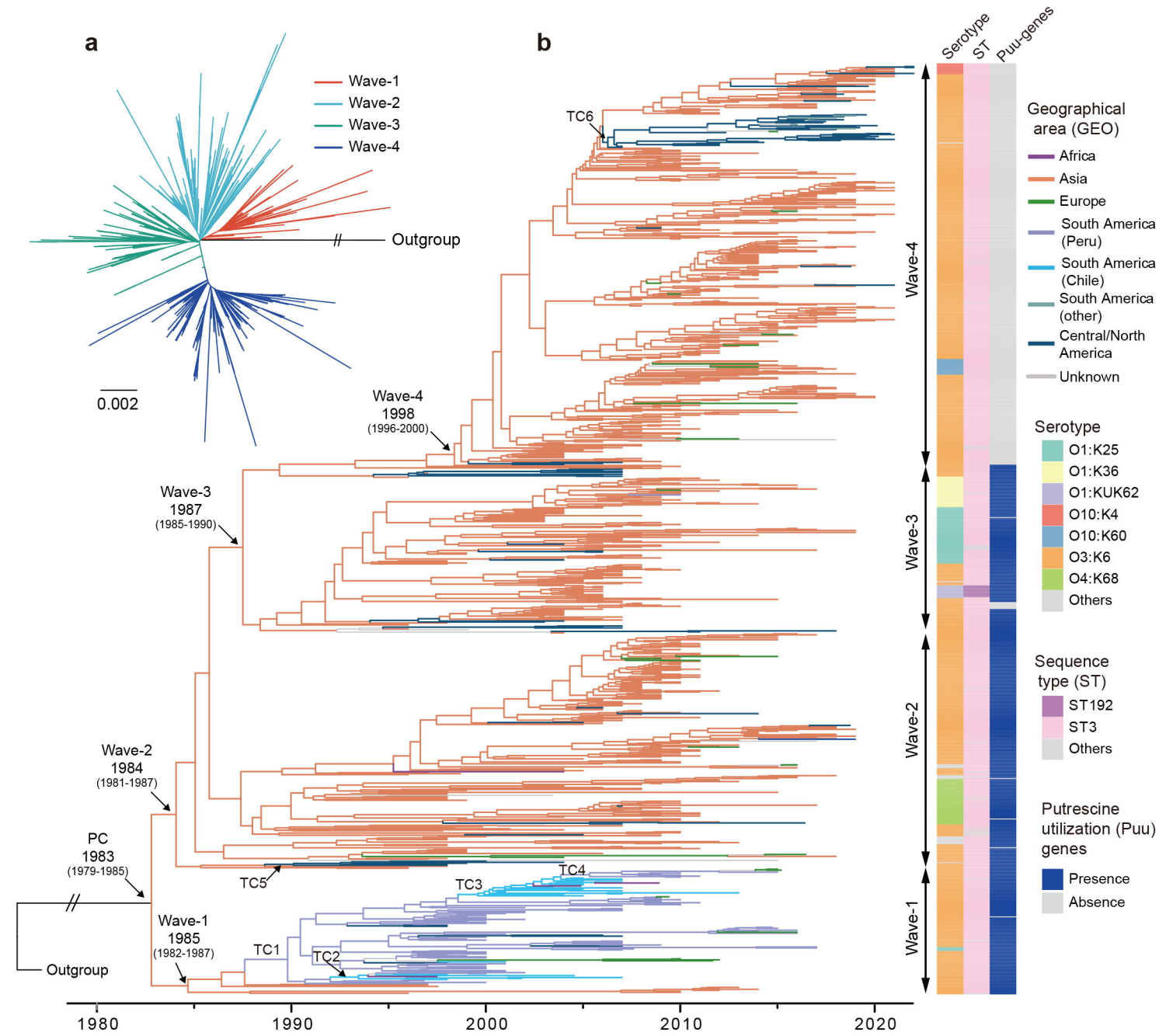
a
Wave-1
Wave-2
Wave-3
Wave-4
Outgroup
0.002
b
Serotype
ST
Puu-genes
TC6
Wave-4
1998
(1996-2000)
Wave-3
1987
(1985-1990)
Wave-2
1984
(1981-1987)
PC
1983
(1979-1985)
Wave-1
1985
(1982-1987)
TC1
TC2
TC3
TC4
TC5
Outgroup
1980
1990
2000
2010
2020
Geographical area (GEO)
Africa
Asia
Europe
South America (Peru)
South America (Chile)
South America (other)
Central/North America
Unknown
Serotype
O1:K25
O1:K36
O1:KUK62
O10:K4
O10:K60
O3:K6
O4:K68
Others
Sequence type (ST)
ST192
ST3
Others
Putrescine utilization (Puu) genes
Presence
Absence

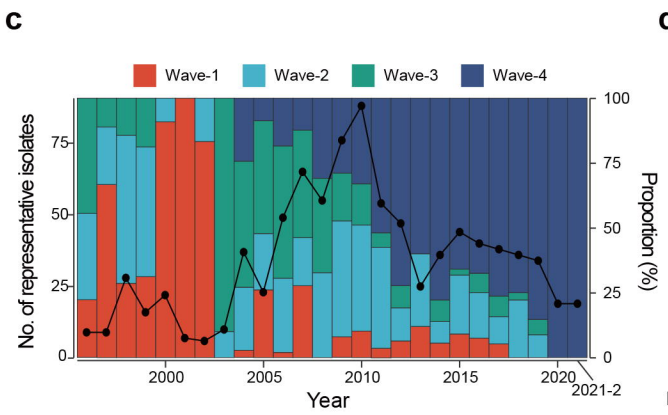
c
Wave-1
Wave-2
Wave-3
Wave-4
No. of representative isolates
Proportion (%)
Year
2021-2

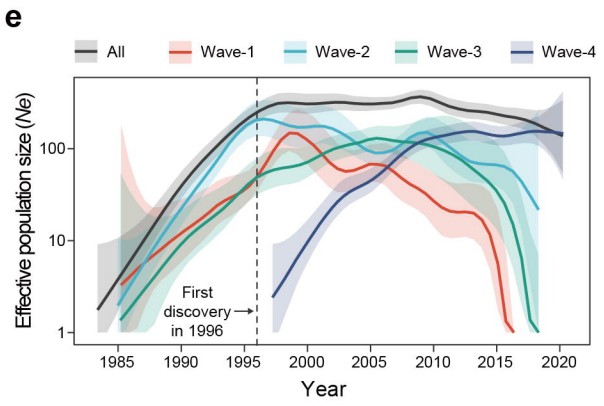
e
All
Wave-1
Wave-2
Wave-3
Wave-4
Effective population size (Ne)
First discovery in 1996
Year

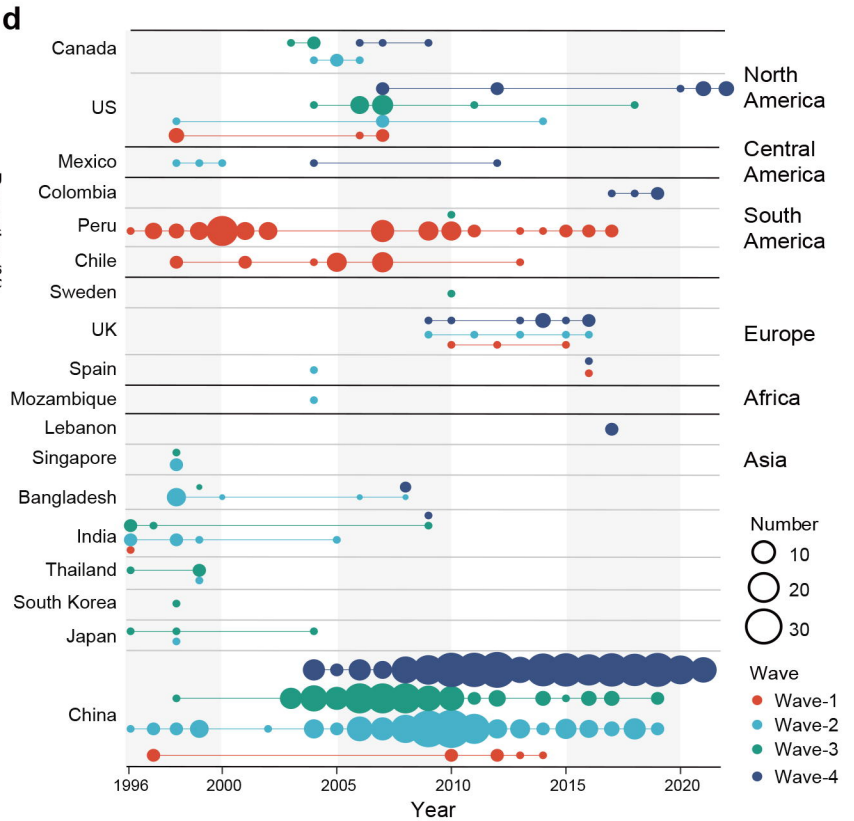
d
Canada
US
Mexico
Colombia
Peru
Chile
Sweden
UK
Spain
Mozambique
Lebanon
Singapore
Bangladesh
India
Thailand
South Korea
Japan
China
North America
Central America
South America
Europe
Africa
Asia
Number
10
20
30
Wave
Wave-1
Wave-2
Wave-3
Wave-4
Year

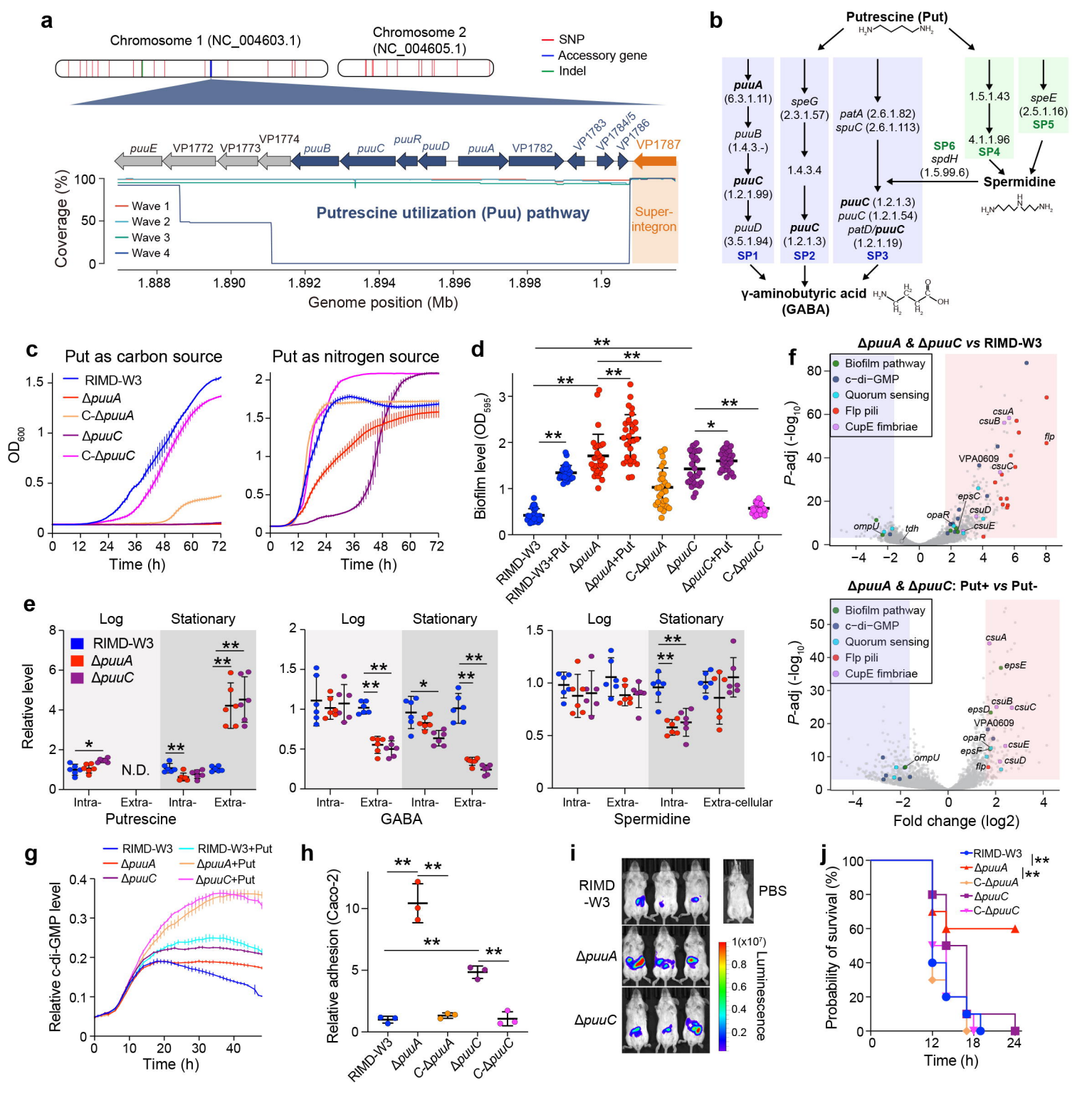
a
Chromosome 1 (NC_004603.1)
Chromosome 2 (NC_004605.1)
SNP
Accessory gene
Indel
puuE
VP1772
VP1773
VP1774
puuB
puuC
puuR
puuD
puuA
VP1782
VP1783
VP1784/5
VP1786
VP1787
Coverage (%)
Wave 1
Wave 2
Wave 3
Wave 4
Putrescine utilization (Puu) pathway
Super-integron
Genome position (Mb)
b
Putrescine (Put)
puuA (6.3.1.11)
puuB (1.4.3.-)
puuC (1.2.1.99)
puuD (3.5.1.94)
SP1
speG (2.3.1.57)
1.4.3.4
puuC (1.2.1.3)
SP2
patA (2.6.1.82)
spuC (2.6.1.113)
puuC (1.2.1.3)
puuC (1.2.1.54)
patD/puuC (1.2.1.19)
SP3
1.5.1.43
4.1.1.96
SP4
speE (2.5.1.16)
SP5
SP6
spdH (1.5.99.6)
Spermidine
γ-aminobutyric acid (GABA)
c
Put as carbon source
Put as nitrogen source
RIMD-W3
ΔpuuA
C-ΔpuuA
ΔpuuC
C-ΔpuuC
OD600
Time (h)
d
Biofilm level (OD595)
RIMD-W3
RIMD-W3+Put
ΔpuuA
ΔpuuA+Put
C-ΔpuuA
ΔpuuC
ΔpuuC+Put
C-ΔpuuC
e
Log
Stationary
RIMD-W3
ΔpuuA
ΔpuuC
Relative level
N.D.
Intra-
Extra-
Putrescine
GABA
Spermidine
Extra-cellular
f
ΔpuuA & ΔpuuC vs RIMD-W3
Biofilm pathway
c-di-GMP
Quorum sensing
Flp pili
CupE fimbriae
P-adj (-log10)
csuA
csuB
flp
VPA0609
csuC
epsC
csuD
opaR
csuE
ompU
tdh
ΔpuuA & ΔpuuC: Put+ vs Put-
epsE
epsD
epsF
Fold change (log2)
g
RIMD-W3
RIMD-W3+Put
ΔpuuA
ΔpuuA+Put
ΔpuuC
ΔpuuC+Put
Relative c-di-GMP level
Time (h)
h
Relative adhesion (Caco-2)
RIMD-W3
ΔpuuA
C-ΔpuuA
ΔpuuC
C-ΔpuuC
i
RIMD-W3
ΔpuuA
ΔpuuC
PBS
1(x10^7)
Luminescence
j
RIMD-W3
ΔpuuA
C-ΔpuuA
ΔpuuC
C-ΔpuuC
Probability of survival (%)
Time (h)

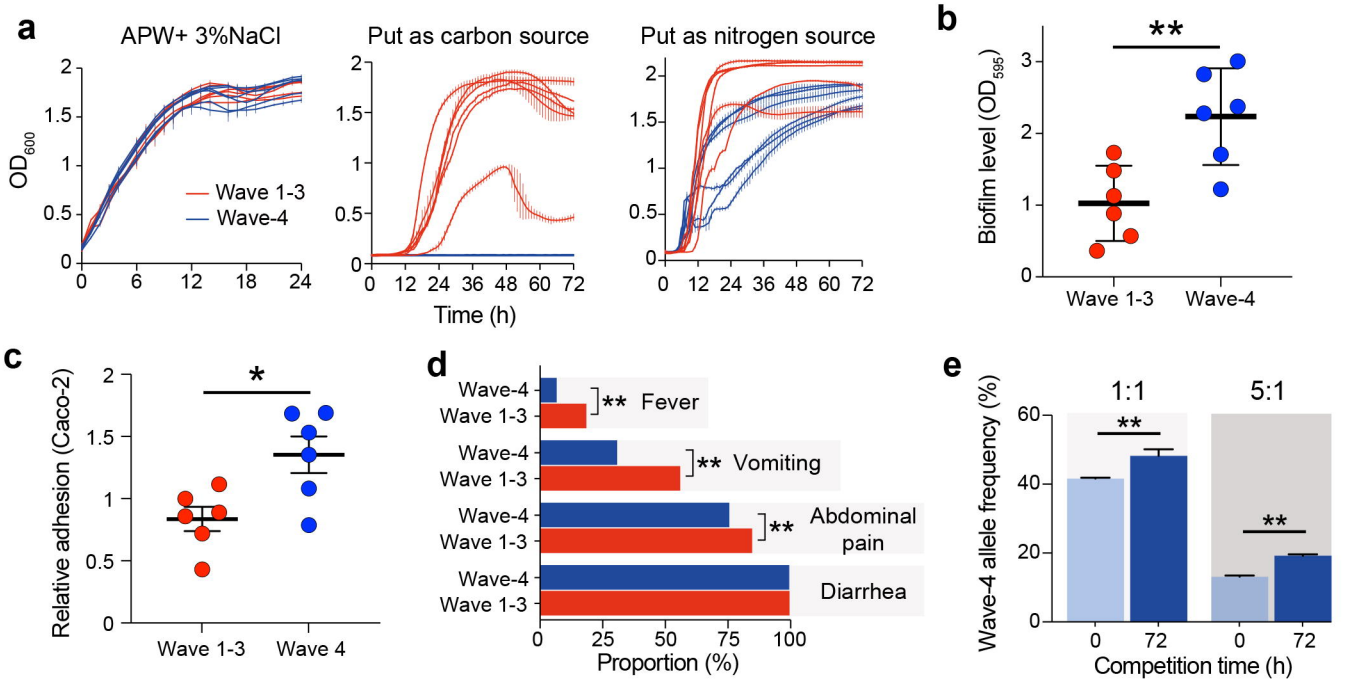
a
APW+ 3%NaCl
Put as carbon source
Put as nitrogen source
OD600
Wave 1-3
Wave-4
Time (h)
b
Biofilm level (OD595)
**
Wave 1-3
Wave-4
c
Relative adhesion (Caco-2)
*
Wave 1-3
Wave 4
d
Wave-4
Wave 1-3
** Fever
** Vomiting
** Abdominal pain
Diarrhea
Proportion (%)
e
1:1
5:1
Wave-4 allele frequency (%)
**
Competition time (h)

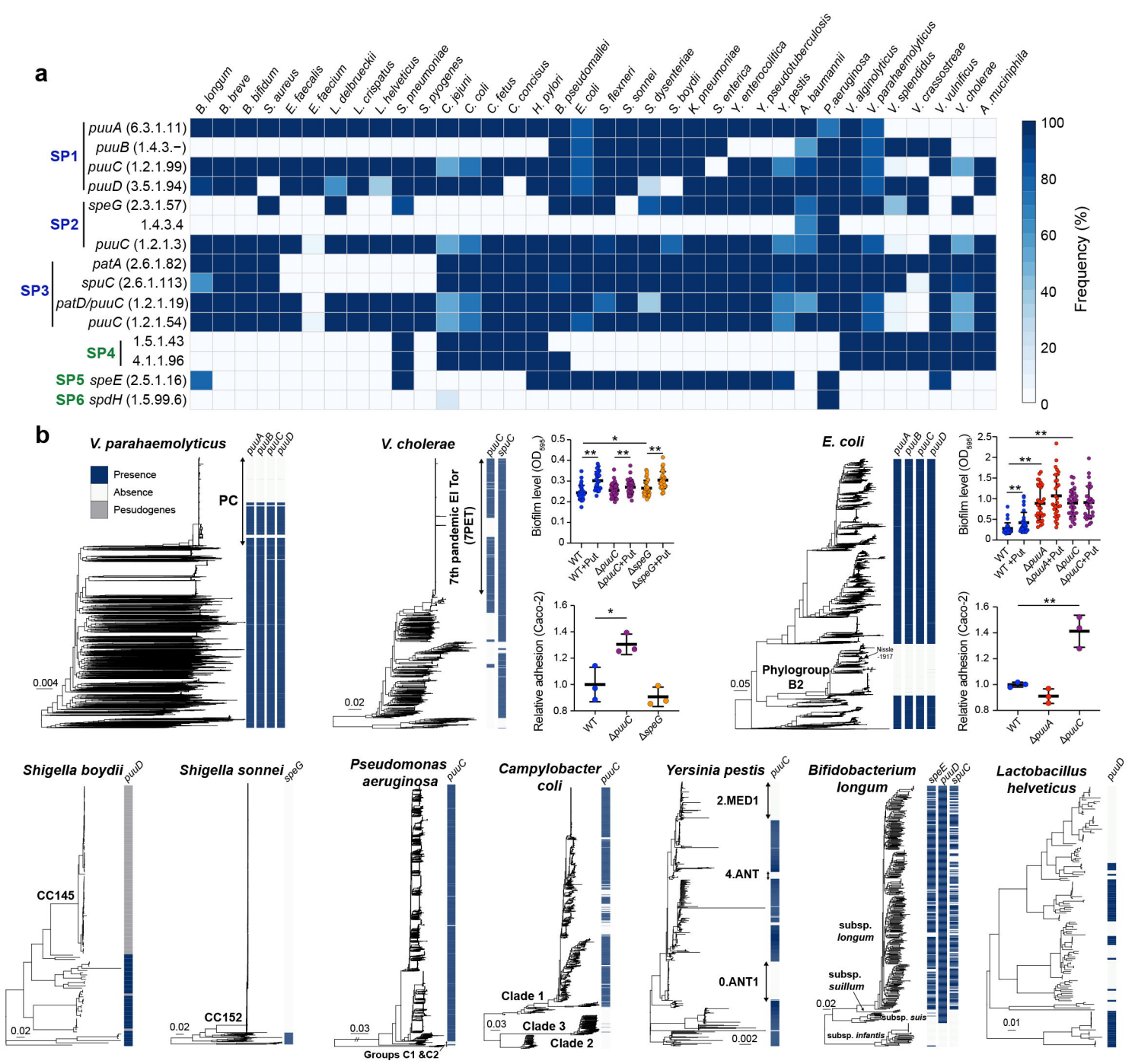
a
B. longum
B. breve
B. bifidum
S. aureus
E. faecalis
E. faecium
L. delbrueckii
L. crispatus
L. helveticus
S. pneumoniae
S. pyogenes
C. jejuni
C. coli
C. fetus
C. concisus
H. pylori
B. pseudomallei
E. coli
S. flexneri
S. sonnei
S. dysenteriae
S. boydii
K. pneumoniae
S. enterica
Y. enterocolitica
Y. pseudotuberculosis
Y. pestis
A. baumannii
P. aeruginosa
V. alginolyticus
V. parahaemolyticus
V. splendidus
V. crassostreae
V. vulnificus
V. cholerae
A. muciniphila
SP1
puuA (6.3.1.11)
puuB (1.4.3.–)
puuC (1.2.1.99)
puuD (3.5.1.94)
SP2
speG (2.3.1.57)
1.4.3.4
puuC (1.2.1.3)
SP3
patA (2.6.1.82)
spuC (2.6.1.113)
patD/puuC (1.2.1.19)
puuC (1.2.1.54)
SP4
1.5.1.43
4.1.1.96
SP5 speE (2.5.1.16)
SP6 spdH (1.5.99.6)
100
80
60
40
20
0
Frequency (%)
b
V. parahaemolyticus
Presence
Absence
Pesudogenes
PC
puuA
puuB
puuC
puuD
0.004
Biofilm level (OD595)
WT
WT+Put
ΔpuuC
ΔpuuC+Put
ΔspeG
ΔspeG+Put
Relative adhesion (Caco-2)
V. cholerae
7th pandemic El Tor (7PET)
spuC
0.02
E. coli
Nissle -1917
Phylogroup B2
0.05
ΔpuuA
ΔpuuA+Put
Shigella boydii
CC145
0.02
Shigella sonnei
CC152
speG
Pseudomonas aeruginosa
Groups C1 &C2
0.03
Campylobacter coli
Clade 1
Clade 3
Clade 2
Yersinia pestis
2.MED1
4.ANT
0.ANT1
0.002
Bifidobacterium longum
subsp. longum
subsp. suillum
subsp. suis
subsp. infantis
Lactobacillus helveticus
0.01